Experimental analysis of time dependent phenomena and temperature effects on macro-synthetic fibre reinforced concretes in different loading conditions

C. Del Prete [*], N. Buratti, C. Mazzotti

Department of Civil, Chemical, Environmental and Materials Engineering (DICAM), University of Bologna, Viale Risorgimento 2, 40136, Bologna, Italy

ABSTRACT

Fibre reinforced concretes (FRCs) are composite materials now largely adopted in structural applications given their mechanical properties in terms of the residual tensile strength, almost absent for plain concrete. The short-term mechanical behaviour of these material has been deeply studied, while their time-dependent deformations have received less attention from the scientific community. The present paper presents the experimental characterization of the creep deformations of a concrete reinforced with polypropylene fibers by means of different types of tests, together with an analysis of the temperature effect. Innovative test set-ups are used to this aim. The paper presents the results of shrinkage, compression creep, uniaxial tension and flexural creep tests and discusses the contribution of the different components of the FRC to the composite creep behavior.

1. Introduction

The well-known brittle behaviour of concrete, often leading to extensive cracking, strongly affects the deformability and the durability of reinforced concrete (RC) structures. To overcome these limitations and possibly reduce the amount of conventional steel rebars, for some decades macro-fibers have been effectively introduced inside concrete, improving its toughness. Fibers, in fact, can control crack propagation trough their bridging mechanism [1] and improve the residual tensile strength.

At the beginning, most of the Fiber Reinforced Concretes (FRCs) were obtained by the addition of steel fibers inside concrete [2]; later, producers exploited the possibility of introducing polymeric fibers [3,4,5], with very good results and diffusion inside the market. More recently, the possibility of using natural fibers has been explored [6,7] even if their diffusion on the market is still very limited.

The large number of experimental campaigns conducted to date, regarding the short term behaviour of the FRCs, allowed to obtain shared protocols and guidelines concerning test procedures and recognized mechanical parameters characterizing the post-cracking behaviour of the composite [8,9,10,11,12,13]. On the other hand, as far as the long-term behaviour of FRCs is concerned, a smaller amount of research works can be found in literature ([14,15,16,17,18]), in spite of its

fundamental importance and considerable complexity. In fact, both the concrete matrix and the fibers can have some viscous behaviour, thus possibly affecting creep and shrinkage of the composite material. In addition, the interface also can play a long-term role in this framework. This is particularly true when considering polymeric fibers, characterized by a viscoelastic nature [19]. In this case, environmental conditions, i.e. temperature and humidity, should also be taken into account [20]. In this regard, with reference to the characterization of fibers, many studies are devoted to analyzing the influence of temperature on the mechanical behaviour of polymers [21,22,23,24,25,26]. An important issue in dealing with the FRC long term behaviour, is the need of standardization of testing procedures ([27,28]), in order to produce results which are comparable and characterized by relevant parameters. Only recently a standard test procedure has been proposed [29] after an extensive round-robin experimental campaign [30,31]. To date, the long-term deformations of FRCs were mostly studied by using flexural tests on prisms [32,33,34,35,28], and in some cases on beams [36,37,38,39]; these procedures do not allow to separate the long-term contribution of the concrete in compression and that of the fibers in tension across the crack. In order to overcome this uncertainty, few studies can be found developing some challenging direct tensile tests. Basically, the specimens used are notched pre-cracked cylinders tested under sustained loads by lever arm systems [40]-[41]. Results are

---

sensitive to the pre-cracking phase and to the distribution of fibres across the notched cross-section. Finally, at a local scale, the long-term contributions of the fibre elongation and slippage, with respect to concrete, can be evaluated with direct tensile tests on single fibers [42,43].

In the present paper, a contribution will be given in terms of experimental approach to separate the different contributions discussed above, especially when dealing with macro-synthetic fibers. At the same time, the proposed approach will be applied to the investigation of the long-term behaviour of macrosyntetic fibers in an environment of variable and increasing temperature. In particular, an articulated experimental campaign is presented concerning a FRC with a unique dosage of polypropylene fibers, 8 kg/m^3, characterised both under short-term and long-term conditions. The long-term tests developed are shrinkage and creep compression tests on cylinders, direct tensile tests on notched cylinders, flexural tests on prisms and direct tensile tests on single fibers.

The results highlight the peculiar aspects in performing creep tests under tensile loads, for example the absence of additional stresses triggered. An innovative set-up to test macro-synthetic fibers in tension is proposed and the results are successful in terms of no damage of the fibre surface and reliability of results compared with the contribution in the other test configuration.

Regarding the fibre elongation, it seems to cover a huge contribution to the entire creep deformation of the MSFRC.

The creep deformations are evaluated considering also the temperature variation, from 20 °C to 40 °C, during the test: this represents a real condition to evaluate the combined effect of the two circumstances, time and temperature. As expected, given the viscoelastic nature of concrete [44] and polymeric fibers [19], both conditions affect the MSFRC response, causing an increment of the deformation.

2. Research significance

The present research concerns the characterization of the time-dependent behaviour of MSFRC coupled with temperature variation. The experimental campaign is developed with two main goals: the characterization of the time and temperature effects on long-term deformations of MSFRCs and, at the same time, the proposal of innovative and optimized set-ups for long-term tests on same materials. Moreover, the measurement and analysis of the creep deformations and their different contributions aim at understanding how the load bearing capacity and others performances of structural elements made of MSFRC could be affected when dealing with the design for the service life, if compared with the short-term counterparts. The MSFRC considered is initially characterized under short-term conditions. Then, long-term tests are carried out under different loading conditions and at different scales, in order to observe the progressively more complex contributions leading to the long-term flexural behaviour. In particular, shrinkage and creep tests are carried out on MSFRC as a composite material, tensile creep tests are carried out on single MS fibers and on MSFRC cracked cylinders and creep flexural tests, on MSFRC prisms. In order to conduct the described tests, some specific set-ups are proposed and validated.

3. Materials and methods

3.1. Materials

The fibre reinforced concrete considered was designed according to the specification for FRCs mixes (EN14845-1:2006 [45]), fine and coarse aggregates are adjusted according to the volume of fibers. The adopted quantities are indicated in Table 1, computed by considering a polypropylene density of 900 kg/m^3. The materials used were: cement type CEM I 52.5R, two types of sand with aggregate size spanning inside the ranges 0 – 1 mm and 0 – 5 mm, gravel characterized by a size range between 5 and 15 mm, potable water and superplasticizer.

The reinforcement consisted of macro fibres made of polypropylene and having a crimped profile (Fig. 1): they are characterized by

Table 1
Concrete admixture.

Concrete component	Quantity
CEM I 52.5 R [kg/m^3]	400
Sand 0–1 mm [kg/m^3]	172
Sand 0–5 mm [kg/m^3]	730
Gravel 5–15 mm [kg/m^3]	837
Water [l/m^3]	184
W/C	0.46
Fibers [kg/m^3]	8.0
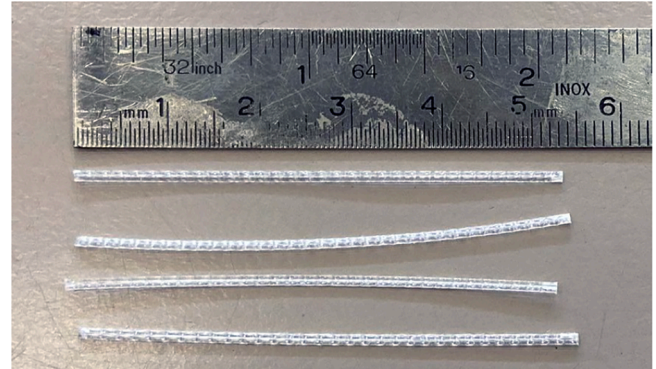
Fig. 1. Polypropylene macro-fibers used.

geometrical and mechanical properties reported in Table 2. They have an irregular cross section and a aspect ratio of 67: some studies showed that these properties can influence the creep deformations of the material, in particular geometry, slenderness and dosage [46].

The FRC was cast using dried aggregates but the water necessary to reach the dry saturated surface (DSS) condition was added during the mixing procedure; aggregates were mixed initially with 50% of water, then the cement and the remaining water was added. Fibers were introduced at the end, with a proper amount of superplasticizer to obtain a slump value of 170 mm.

3.2. Experimental campaign

In order to identify and evaluate the viscous contribution of each component to the overall long-term behaviour of macro-synthetic FRC (MSFRC) elements under flexure, a sequence of long-term tests was designed so that results were made available from the material behaviour to the structural counterpart, with a complete coherence. In particular, a three-steps approach was adopted: i) in the first step long-term tests on materials were performed, in the form of of shrinkage and creep compression tests on concrete cylinders and tensile tests on single fibers; ii) in the second step, the tensile behaviour of fibres was coupled with the bond and investigated trough long-term uniaxial tensile tests on MSFRC notched cylinders; iii) the contributions by concrete in compression and by fibers in tension were considered together by performing long-term flexural tests on MSFRC prisms. All the long-term

Table 2
Macro-synthetic fibre properties.

Fibre property	Unit	Value
Fibre length	[mm]	54
Fibre diameter	[mm]	0.81
Fibre Aspect ratio	[-]	67
Fibre material*		PP
Mean fibre tensile strength	[MPa]	473
Elastic secant modulus*	[GPa]	5.7–6.3
Shape		straight crimped

* As declared by the producer

tests were carried out with a given sequence of temperature variations with time. Since the focus of the study was related to the investigation of the different mechanisms connected to the fibres presence, all the FRC specimens tested under sustained load (tensile and flexural) were pre-cracked, thus activating the fibers contribution.

The short-term material properties of the materials were measured by following the same approach but with standard short-term flexural (EN14651-[8]) and compressive tests (UNI EN 12390–3-[47]) at room temperature (23 °C). The elastic modulus of concrete was also measured (UNI EN 12390–13-[48]).

3.3. Specimens preparation

Different types of specimens were used for the different types of tests previously described. In particular, elastic modulus, shrinkage and creep compression deformations were measured on standard 150 mm × 300 mm (diameter × height) cylinders, which were properly rectified before the tests.

Long-term tests on single fibres were carried out on the same fibers introduced in the concrete matrix. The free length (L_e) of the specimens during the tests was 23 mm.

Long-term uniaxial tensile tests on the MSFRC were carried out on notched cylinders. Since they were intended to represent the tensile portion of the cross section of prism in bending; these cylinders were cored from standard prisms along their longitudinal direction (Fig. 2), in order to maintain a consistent orientation of fibers [49]. In order to make these specimens, five 150 mm × 150 mm × 600 mm prisms were cast, then cut into three equal cubes each of which was then cored, obtaining 125 mm × 150 mm (diameter × height) cylinders that were subsequently notched at mid height for a depth of 10 mm. Before notching steel plates were glued to the end sections of the cylinders and later used in order to attach the specimens on the testing machine.

The flexural tests were performed on 150 mm × 150 mm × 600 mm notched prisms, whose dimensions were set according to the EN14651 [8]. Table 3 shows the type of adopted specimens, their number, dimensions and type of test.

3.4. Test set-up and instrumentation

In this section, the experimental set-up and the procedures adopted are described in detail for the different tests introduced before. They were carefully designed in order to mainly assure the undamaged condition of the specimens when they were mounted and subsequently loaded and, on the other hand, to avoid the triggering of unexpected mechanisms.

As specified before, tests were performed under environmental controlled conditions in a climatic chamber with a constant relative humidity of 55% and an initial temperature of 20 °C which was increased by 10 °C after 50 and 120 days, reaching a final value of 40 °C. The duration of the time interval with a given assigned temperature was roughly defined so to obtain an approximate constant rate of increase of

Table 3
Outline of the number and specimen type, their dimensions and the type of test realized.

Type of test	Specimen type	N° of specimens	Dimensions
Elastic Modulus	Cylinder	2	d = 150 mm h = 300 mm
Shrinkage	Cylinder	2	d = 150 mm h = 300 mm
Compression creep	Cylinder	2	d = 150 mm h = 300 mm
Flexural creep	Notched Prism	8	section = 150 × 150 mm²length = 600 mm
Uniaxial tension creep	Notched cored cylinder	12	d = 125 mm h = 150 mm
Uniaxial tension creep	Fiber	4	L_e = 23 mm

the measured quantities.

3.4.1. Shrinkage test
Total shrinkage strain was measured on two cylindrical specimens without any load applied, the samples were placed in the climate controlled chamber and their deformation was monitored by using two 60 mm long strain gauges for each sample, glued at circumferential distance of 180 °C. They were placed along the vertical axis of the cylinder (Fig. 3).

3.4.2. Creep compressive test
Fig. 4 shows the frame used for the creep compression test. The loading frame is composed by two steel plates, connected by four threaded steel bars positioned at the corners. The load is generated by

Fig. 3. Cylinders prepared for shrinkage tests in climate room.

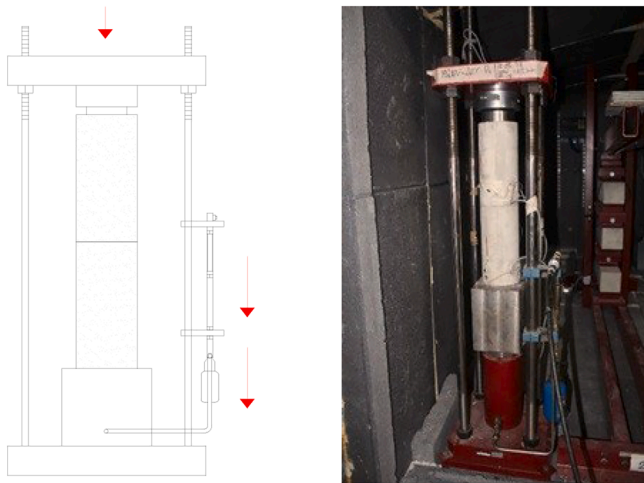**Fig. 2.** Preparation of the cylinders used for the creep tensile tests.

Fig. 4. Test set-up for creep compression tests.

means of a hydraulic jack, whose oil pressure variations with time are compensated by an oil accumulator. The samples tested were two cylinders (Fig. 4) housed between the two steel plates. During the creep tests the applied load was a percentage (20%) of the maximum compression strength, to simulate service conditions. The creep test duration was 300 days and at the end of this period the specimens were unloaded and the recovered deformations were measured for further 30 days. During the tests strains were measured as described in Section 2.4.1.

3.4.3. Fiber tensile creep test

Single macro-synthetic fibers were subjected to creep tests by means of a properly developed system. The experimental procedure carried out in two main phases. In the first, eleven macro-fibers were tented in tension, by using a 500 kN universal machine properly equipped with an additional load cell with 2 kN capacity (Fig. 5). MS fibers were clamped at both ends with pairs of aluminium plates (Fig. 5a), equipped with sand paper glued on their internal sides, in order to avoid relative displacements between the element tested and the plates. Tests were carried out under displacement control, with a stroke velocity of 5 mm/min and until the breakage of the fibers (Fig. 5b).

In the second phase, tensile creep tests on single fibers were carried out, by using the steel frames in Fig. 6a. To ensure a proper stability of the long-term load with time, a lever-arm system based on gravity loads was used. In particular, each system is composed of a steel base plate and two vertical C-profiles supporting a top horizontal lever. The fiber

Fig. 5. (a) Setup of the tensile test on single fibre and (b) fibre at failure.

extremities were mechanically gripped inside two small steel cylinders with sand paper (Fig. 6b) and the whole assembly was placed vertically under the edge of the small arm of the lever system: the lower cylinder was, then, screwed to the base plate while the upper was connected through a pin to another larger cylinder, the latter being hinged to the smaller lever arm through a further pin orthogonal to the previous one (Fig. 6c).

In order to control if possible fibers slippage from the cylinders occurred during the long-term tests, the extremities of the free portion of filament entering the cylinders were marked with white paint at the beginning of the test and regular observations with an optical scope were done during the loading period. No appreciable slips were recorded. It is important to notice that the gripping system proposed for long-term tests, was already adopted and tuned for instantaneous pull-out tests (see experimental campaign described in [50]) and for instantaneous tensile tests on single fibers, where reliability of results has been already assessed. In the former case, the shape of the force–displacement curves allowed to exclude the triggering of slippage at the fibre-sand paper interface [50].

Two different long-term stress levels were applied during the creep tests to two groups of samples, namely 20% and 40% of the mean tensile strength obtained from the instantaneous tests, in order to investigate the different viscoelastic response. The elongation of each fibre was monitored during the test by using two LVDTs (10 mm stroke) fixed to the upper cylinder through an aluminium support (Fig. 6c). The longitudinal deformation of the filament was obtained by dividing the measured elongation by its free length (distance from cylinder to cylinder).

3.4.4. FRC cylinders tensile creep test

The long-term behaviour of notched cylinders under uniaxial tensile load was observed by following an experimental procedure, organized according to three phases: pre-cracking, creep test and evaluation of residual capacity. The first and last phases involved instantaneous tests at room temperature while the creep stage presented a sustained load applied under assigned environmental conditions.

In order to apply the tensile force to the notched cylinders (see section 2.3) during the different tests, the two steel plates glued at their ends were used. The pre-cracking phase was carried out by connecting the steel plates to the upper and lower grip system of a universal testing machine (the same as per section 2.4.3) through articulated joints allowing for rotations, so that no additional stresses were induced when the tensile load was applied (Fig. 7a). Furthermore, these boundary conditions are consistent with those in the creep tests, described in the following.

Tests were carried out under crack opening control, measured by means of three clip on displacement (COD) transducers placed at equal radial distance of 120° across the notch (Fig. 7b). During the test the following COD rates were used, 0.005 mm/min, for $COD_m < 0.05$ mm and 0.01 mm/min until a COD_m value of 0.3 mm where COD_m indicates the mean COD value, computed from the measurements of the three transducers. The target value of the mean COD at the end of the pre-cracking phase, i.e. 0.3 mm, was defined considering the mean crack opening over the height of the cracked section of prims in three-point bending tests at CMOD = 0.5 mm (see Section 4.5), i.e. approximately 0.2 mm, and the results of preliminary uniaxial tension tests that showed that for COD < 0.3 mm part of the notched section of the specimens was not cracked (see also Section 3.4).

Specimens were then unloaded. Given the uneven distribution of both the tensile strength of concrete and, most importantly, of fibres, the crack opening was not uniform around the perimeter of the cylinders, thus introducing non-uniform behaviour of fibers in different areas of some cylinders. After the pre-cracking phase, three cylinders out of fifteen were selected based on the maximum residual tensile strength at 0.3 mm of crack opening and on the minimum difference between crack opening values coming from the three COD sensors.
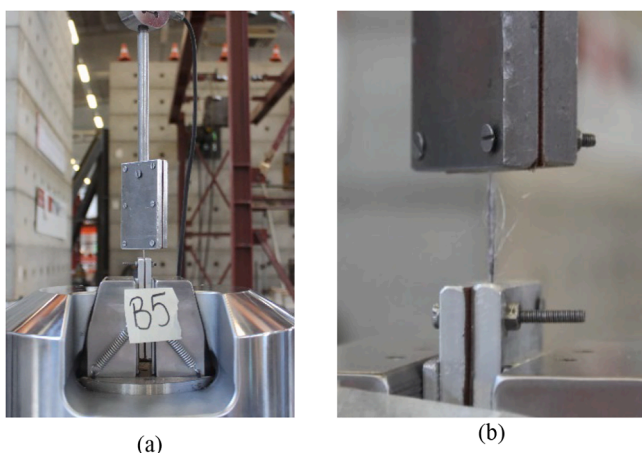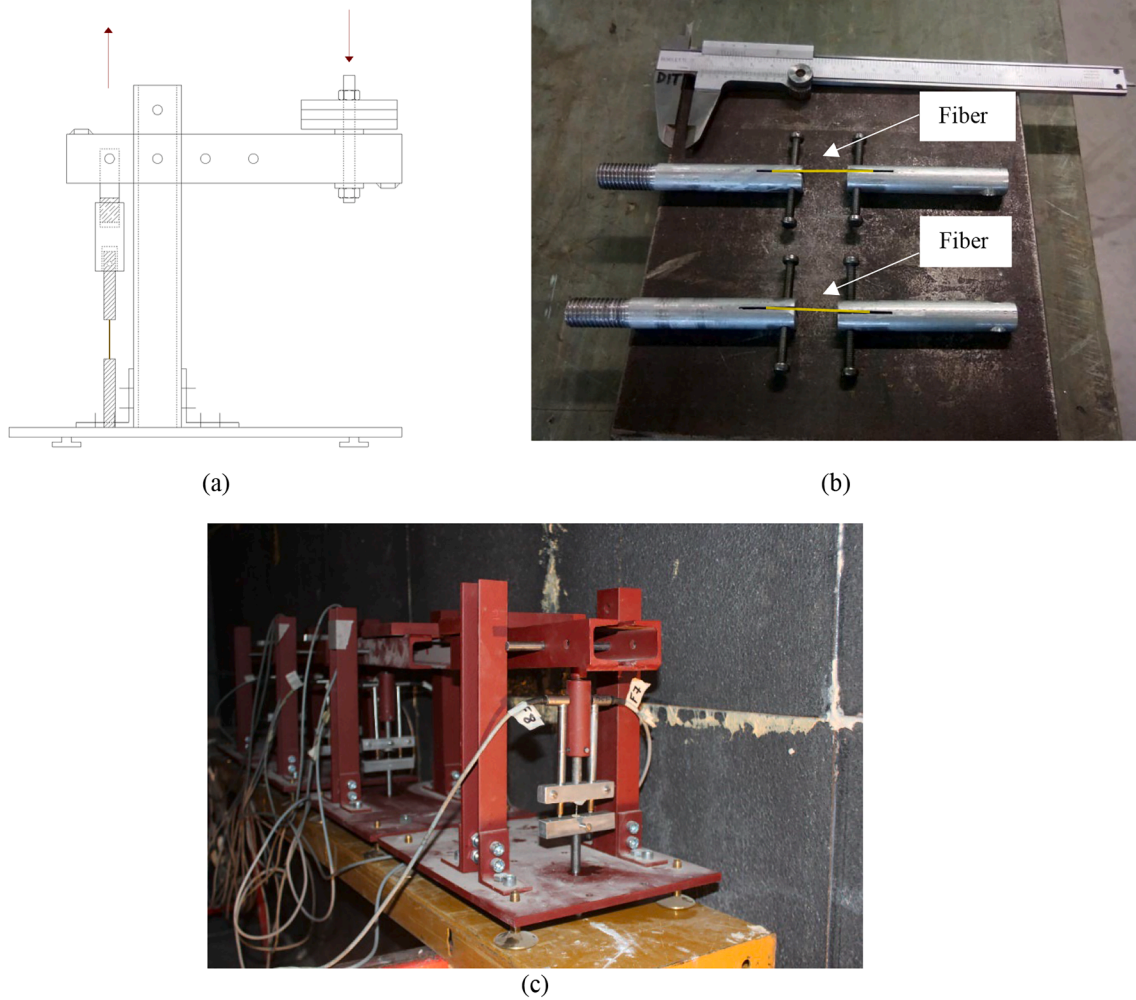
(a)

(b)

(c)

Fig. 6. Tensile creep test on a single fibre: (a) Frames to test fibers under creep load; (b) Detail of aluminium supports where fiber and sand paper is allocated; (c) Steel frames for creep tensile tests on fibers.
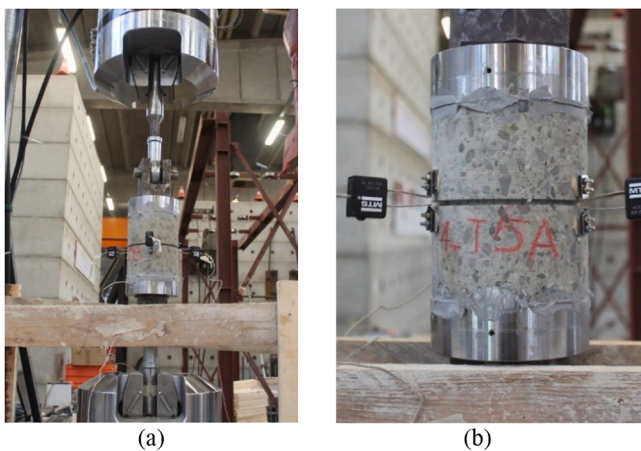

(a)   (b)

Fig. 7. Pre-cracking phase of cylinder under uniaxial tensile load and crack opening measured by COD at 120° radial distance.

Fig. 8. Lever system for creep tensile test on MSFRC cylinders.

The creep tensile test on notched cylinder was created according using a first type lever-system, with a swinging horizontal arm hinged at the top of a steel column (Fig. 8). In order to test more cylinders within the same system, three of them were mutually connected by means of
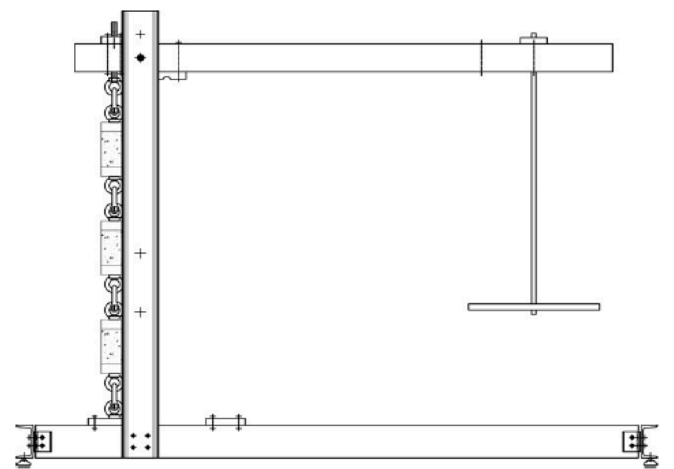
eyebolts, screwed to the steel plates at their ends, and shackles, forming a long "chain" (Fig. 9a) where each cylinder was only subjected to pure tension (free rotation capability - Fig. 9b). The "chain" was vertically placed at the extremity of the short arm of the lever system and was connected by means of a bolt; similarly, it was also bolted to the lower
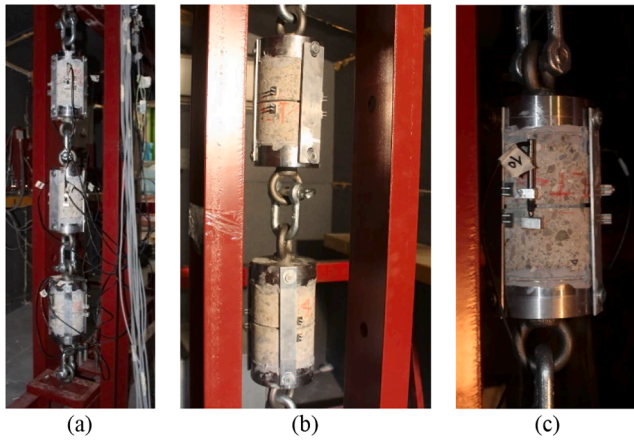
Fig. 9. Tensile creep test: (a) Chain of three cylinders under uniaxial tensile load; (b) Detail of two cylinders of the loaded chain; (c) LVDT to measure the crack-opening.

Fig. 10. Pre-cracking phase in three point configuration.

horizontal steel support (Fig. 8). The creation and placement of the "chain" needed particular care since the cracked condition of the cylinders made them prone to spontaneously increase the crack opening during the process. To this purpose, three aluminium bars (120° apart) were bolted to the steel plates at the extremities of each cylinder to keep its crack opening constant until the starting of the long-term test. Once the "chain" was properly placed, the bolts were partially released but the bars were not removed, in order to prevent a possible catastrophic failure if a single cylinder broke (Fig. 9b). Cylinders were stacked according to the criteria of decreasing residual strength, starting from the top of the "chain". It should be noticed that the cylinders are free to rotate at their ends as in the pre-cracking test setup.

The tensile force in the "chain" was generated by applying gravity loads at the end of the longer lever arm. The applied long-term stress was approximately 50% of the residual strength measured at 0.3 mm of instantaneous crack opening; each cylinder of the "chain", in fact, had a slightly different long-term stress/residual strength ratio since the residual strength was different for each one of them. In the calculation of the ratio, the effect of the weight of the items suspended above the actual cylinder was considered. During the tensile creep test, the crack opening of each cylinder was monitored by using three vertical LVDTs placed, 120° apart, across the crack (Fig. 9c).

At the end of the period of sustained load, cylinders were unloaded and the crack opening was measured for further 30 days, in order to observe the potential crack opening recovery.

The last phase of the process consisted in testing each cylinder in tension, until failure; to this purpose, the same loading equipment and procedure considered during the pre-cracking phase (Fig. 7) was used.

3.4.5. Flexural creep test

The methodology used in case of flexural creep tests shared the approach of the previous ones and was developed again into three phases: pre-cracking, long-term test and short-term failure.

The pre-cracking tests were performed in a three-point bending configuration (Fig. 10), according to EN14651, by using a 500 kN universal testing machine. Tests were carried out in crack mouth opening displacement (CMOD) control until a crack opening value of 0.5 mm, corresponding to the residual flexural strength f_{R1}, followed by a total unloading which led to the measurement of the residual crack opening. After the pre-cracking phase, three out of eight specimens were selected according to the criteria of the higher residual tensile strength at CMOD = 0.5 mm.

In order to perform the flexural creep tests, a steel frame based on a lever mechanism of 2° type was developed (fulcrum is external to the
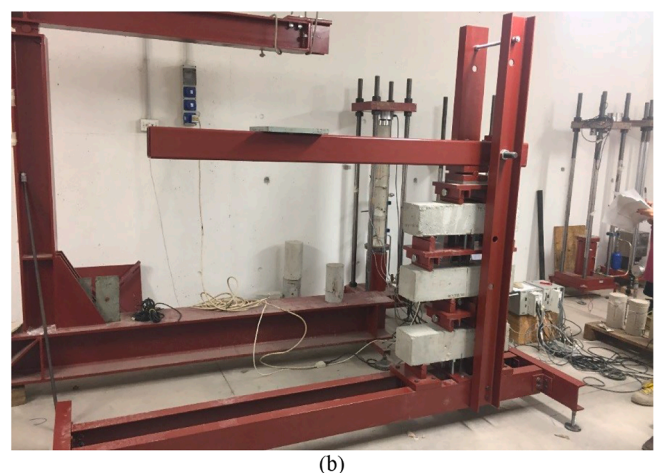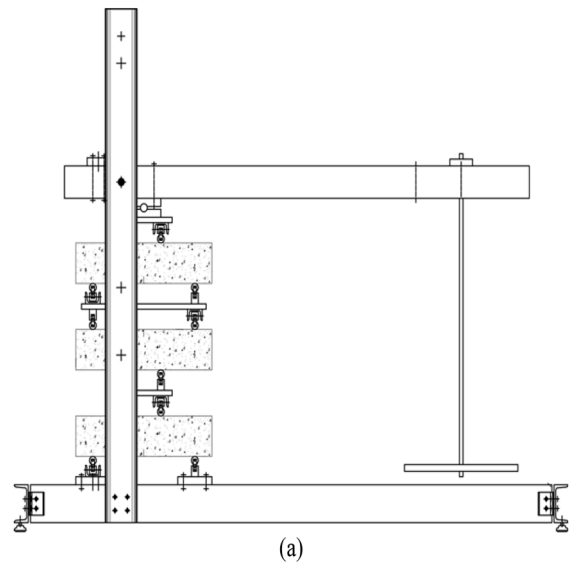

(a)

(b)

Fig. 11. Flexural creep test set-up based on lever arm of 2° type.

two forces application points – Fig. 11); in more details, the fixed part of the system is composed of a horizontal double C beam sustaining a vertical twin column; the horizontal lever is hinged in-between the two half columns and on top of them. It is kept in the horizontal position by the stack of specimens, to which a vertical force is transmitted. Each frame can host three specimens, properly stacked according to the scheme shown in Fig. 11: each prismatic specimen is vertically separated from the others by means of steel plates, equipped with two cylindrical rollers on each side. The span between the rollers is different on opposite sides of each specimen (Fig. 11b), so that the load is applied to the prisms according to four-point bending configuration; the long span is 450 mm while the short span is 150 mm ([51,52]). In any pair of rollers, one is also hinged around the longitudinal axis of the prism, so that torsional moments are avoided. The arrangement described, requires adjacent prisms to be rotated on opposite sides and in order to reduce, as much as possible, the difference between forces applied to each specimen, the stacking order followed the criteria the higher the residual strength, the lower the position in the stack. In fact, each prism had a growing dead weight applied, going down the stack. In order to produce an additional vertical force on top of the stack of specimens, a calibrated number of steel plates was positioned at the far extremity of the horizontal lever (Fig. 11). The intensity of the applied sustained load was computed by considering 50% of the residual flexural strength, where also the weight of the additional steel plates was included. It should be noticed that this load rate was defined based on pre-cracking tests carried out at room temperature.

In order to measure the CMOD during the test, one 2 mm stroke LVDT was positioned across the notch of each prism. Since the longitudinal axis of the LVDT was at a distance of 5 mm from the surface of the prism, in the results this issue was considered by reducing the LVDT measurement of a factor $\delta = h/(h + y) = 150/(150 + 5)$ (being h = total depth of the specimen, y = distance from LVDT to bottom surface of the prism), as claimed in EN14651 [8]. The calculation was made by considering that the crack was already formed and that the point of rotation of the two halves of the prism was likely localized at the top of the compression chord.

At the end of the period of sustained load, whose duration was about 300 days, prisms were completely unloaded and the CMOD was measured for further 30 days, in order to observe the potential crack opening recovery. The removal of the specimens from the frames was carried out with particular care and by rotating the prisms of 90° around their longitudinal axis.

Finally, all the considered prisms, both previously subjected or not to long-term loading, were tested under short-term loading until a CMOD of 4 mm, according to EN14651. In this way, the possible influence of the sustained load on the residual capacity of the system was assessed.

4. Experimental results

4.1. Shrinkage deformation

Fig. 12a shows the shrinkage deformations of the two specimens tested (black solid lines): the horizontal black harrows identify the time interval during which the temperature was kept constant at 20°, 30° and 40° C. Since the deformations correlated to shrinkage induced a volume reduction while the temperature increment induced a sudden expansion, the profile of the strain curve had a vertical jump at 50 days and 175 days, when the temperature was increased from 20° to 30 °C and from 30 °C to 40 °C, respectively. The global trend of the curves was soon recovered in the weeks following the temperature change. Irrespective of the temperature variations, the global shrinkage development presented a rough continuity, with its slope reducing with time due to smaller velocity of water consumption and evaporation. Small irregularities of the curves came from small unpredicted variations of temperature and humidity inside the climate chamber. The observed results suggested that the considered concrete provided a predictable shrinkage; in fact, according to the EC2 shrinkage model [53], the analytical value after 50 days should be 521 µε while, after 300 days, approximately 630 µε, without considering the deformations induced by the change of temperature.

4.2. Creep compression deformation

The FRC tested was characterized by a compressive strength of 55 MPa and elastic modulus of 29.5 GPa (assessed by tests on cylinders). The results are presented in terms of curves deformation and creep coefficient vs time measured from the load application time: the elastic deformation is calculated right after the load application (ε_{inst}). The load application procedure took less then 60 s.

Fig. 12a showed the total deformations provided by the cylinders subjected to creep tests (red curves), including also the creep recovery after unloading. These curves also include the shrinkage contribution, which was subtracted in order to obtain the creep deformation only. From this deformation, the creep coefficient – $\varphi_c = (\varepsilon_{visc} - \varepsilon_{inst})/\varepsilon_{inst}$ – was evaluated (Fig. 12b), allowing to observe the long-term behaviour due to the applied stress with variable temperature. The global envelope confirmed the general trend expected for the creep: a monotonic increase of deformation with time but at a decreasing rate; on the contrary, after each temperature increment the slope of the curves quickly recovered but this recover was smaller with time. The resulting creep coefficient after more than 9 months of sustained load was similar to that analytically computed according to EC2 [53] and equal to 1.75. Finally, by comparing the deformations instantaneously recovered during the
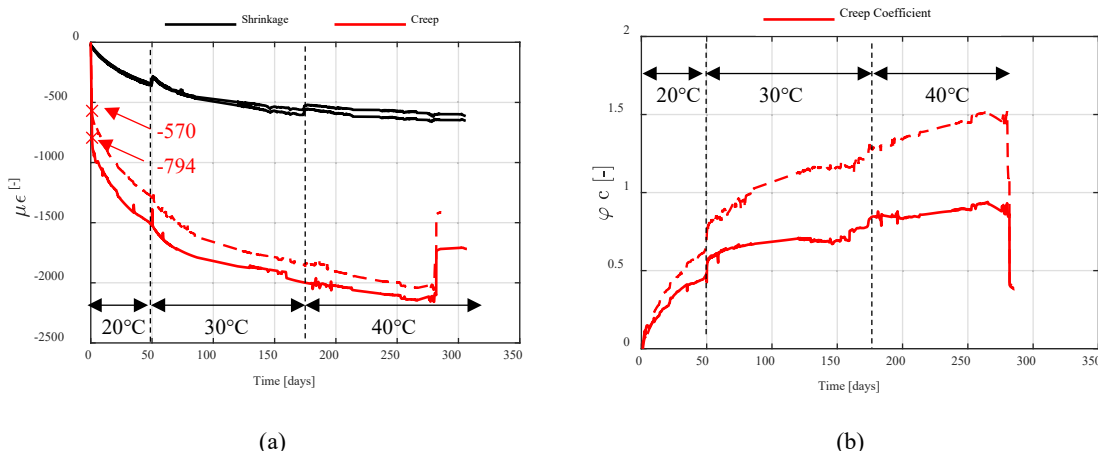

(a)   (b)

Fig. 12. (*a*) Drying creep in compression and Shrinkage deformation (µε) and (*b*) creep coefficient development with time.

unloading with those measured during the load application, they appeared to be consistent (mean value of 509 με vs 615 με – Fig. 12a), even if a reduction can be observed due to aging of concrete.

4.3. Tensile creep deformation of single fibers

Before the long-term tests, an instantaneous characterization of the mechanical behaviour of fibres under traction was carried out, and an example of the corresponding stress–strain diagram is reported in Fig. 13. From the curves, the peak tensile strength and secant elastic modulus at peak were extracted. The outcomes of the long-term tests were presented in terms of strain evolution vs time in Fig. 14a and 14b, for fibers subjected to 20% and 40% of their tensile strength (defined as load ratio), respectively. Two fibers for each case were tested. Results concerning load ratio of 40% showed a shorter time under load and the first time period at a temperature of 20° is lacking; this is because of a late beginning of these tests, even though they were conducted in parallel with the other tests and inside the same climate chamber. The first aspect which can be noticed is the reduced scattering of results from the two fibers subjected to the same load condition; this remark suggested that the number of tested fibers, even if limited, was still representative.

Examining the initial instantaneous deformations at the loading time, values were consistent since the deformation ε exhibited by the fibres with higher applied load was approximately 2.2 times the value ε exhibited by the fibres with lower load.

The long-term behaviour, as expected, showed a decreasing slope of the curve with time while the opposite can be observed when the temperature was increased. At higher load ratio (40%) the latter slope increment was larger with respect to that occurred with the same temperature increase but at lower load ratio, meaning that the two parameters can play a coupling effect.

Fig. 15a and 15b showed the development with time of the creep coefficient $\varphi_{fib} = (\varepsilon_{visc} - \varepsilon_{inst}) / \varepsilon_{inst}$, respectively for load ratios of 20 and 40%, computed considering an elastic deformation computed as described in the previous section 3.2. Creep coefficients spanning from 1.8 to 2.3 and 2.1–2.3 were obtained for load ratios of 20% and 40%, respectively.

4.4. Tensile creep deformation of cracked cylinders

The cylinders tested were named T3A, T5A, T3C, where the number represented the prism of origin while the last letter referred to the portion of prism from which they were cored (A and C were lateral portions while B was that in the middle).

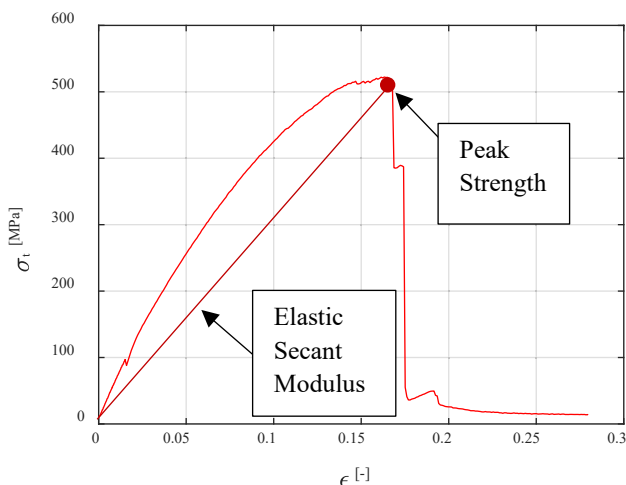According to the procedure described in section 2.3, twelve cylinders

Fig. 13. Stress – strain curve of a fibre direct tensile test.

were produced and, then, pre-cracked: among these, three were selected according to the higher residual strength measured and the crack opening development along the three directions (Table 4). As an example, Fig. 16 showed the tensile force vs crack opening displacement (COD) curves measured from two cylinders during the pre-cracking phase: black dashed curves corresponded to the opening read from each LVDT while the red solid curve represented the mean response. In particular, the T3C sample (Fig. 16a) was an example of not uniform opening of the crack since, on one side, the elongation is noticeably higher than that on the others, although no parts of the specimens had negative deformations (compression). On the contrary, the sample T5A (Fig. 16b) showed an almost uniform opening along the three directions 120° apart. Although the non-uniform behaviour, the sample T3C was used for the creep test, as to investigate the creep response of a specimen characterized by a different behaviour: it is important to remark that, despite the non-uniform crack-opening, the cylinder selected did not show portions in compression during the test. In Table 4, the COV for the COD values measured from each cylinder used are indicated.

Fig. 18 and Fig. 19 showed the COD and creep coefficient – $\varphi_t = (\varepsilon_{visc} - \varepsilon_{inst}) / \varepsilon_{inst}$ – development with time, whose calculation considers the elastic deformation (ε_{inst}) evaluated after the load application. They increased with time at a reducing rate but when the temperature was increased, a sudden rate increment was observed. This latter effect faded with time, suggesting that most probably the increment of deformation under sustained load tends to reach an asymptotic value even at moderate level of temperature but constant for long period of time (50 days, 125 days, 105 days). estimated in terms of slope, equal to 1.2% when passing from 20 °C to 30 °C and 0.4%, from 30 °C to 40 °C.

As expected, sample T3C exhibited the larger instantaneous elongation when loaded and the larger long-term COD; in fact, the same sample provided also the larger residual COD and scattering of results (non-uniform crack opening) during the pre-cracking phase. This behaviour can be attributed to an irregular distribution of fibers across the cracked surface, as can be seen in Fig. 17, leading to stresses strongly variable among different fibers. Despite this, no failure was observed.

Under long-term loading condition, the contribution to the deformation was given by the fibres elongation and by the fibre-concrete interface slippage. In particular, the progressive elongation of fibres with time, led to the reduction of their cross-section, due to the Poisson effect, which weakened the long-term bond capacity, since fibers could possibly detach locally by the surrounding concrete [54]; this would be more apparent in the portion of fibre close to the crack, since there the fibre stress was higher. When the bond loses its effectiveness, the active bonded length moved backword along the fiber, by increasing the fibre unbonded length and the corresponding long-term elongation. In conclusion, results from tensile creep tests on cracked cylinders included both contributions of fibre creep and weakening of interface behaviour, which could also be considered like a long-term slip.

After the conclusion of creep tests, the specimens were unloaded (this phase corresponds to the COD drop in Fig. 18-Fig. 19) and the COD was recorded for 30 more days, until values appeared stable. The deformation values at the end of the test represented the residual COD while the elastic contribute was recovered. Also, for these tests the elastic deformations used to compute the creep coefficients are calculated right after the load application. After that period of time, each specimen was subjected to "instantaneous" tensile test until failure. The three phases, pre-cracking, creep and failure, were then merged in one single curve for each sample in term of COD, by considering that the final point of the curve coming from the previous phase was the starting point of the following one. Fig. 20 showed all the assembled tensile force-COD experimental curves, superimposed to an ideal curve (black solid line) enveloping the three phases: it characterizes the long-term behaviour in tension of the FRC tested.

In Table 4 is indicated, for the three cylinders tested, the number of fibers counted on the cracked surface after the specimens have been tested until failure.
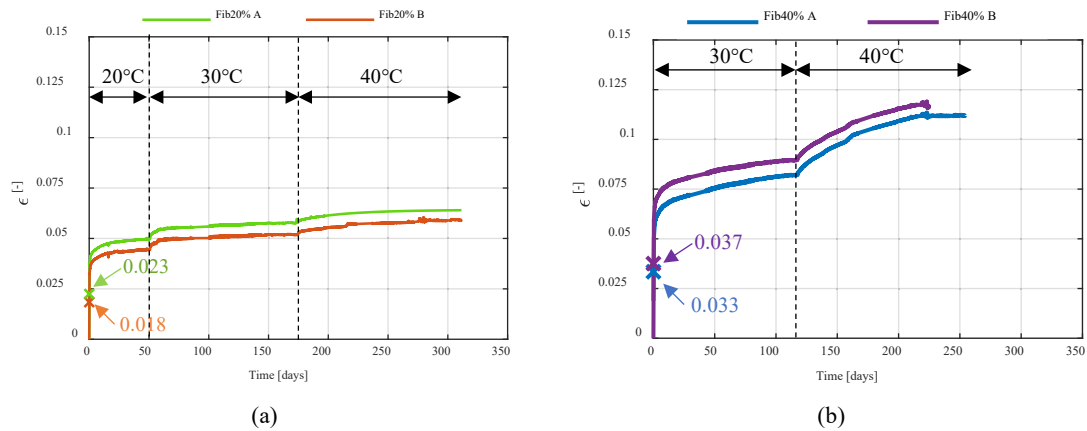
Fig. 14. Fibre tensile creep test: Strain – time relation for fibers (a) loaded at 20% and (b) 40% of the tensile strength.
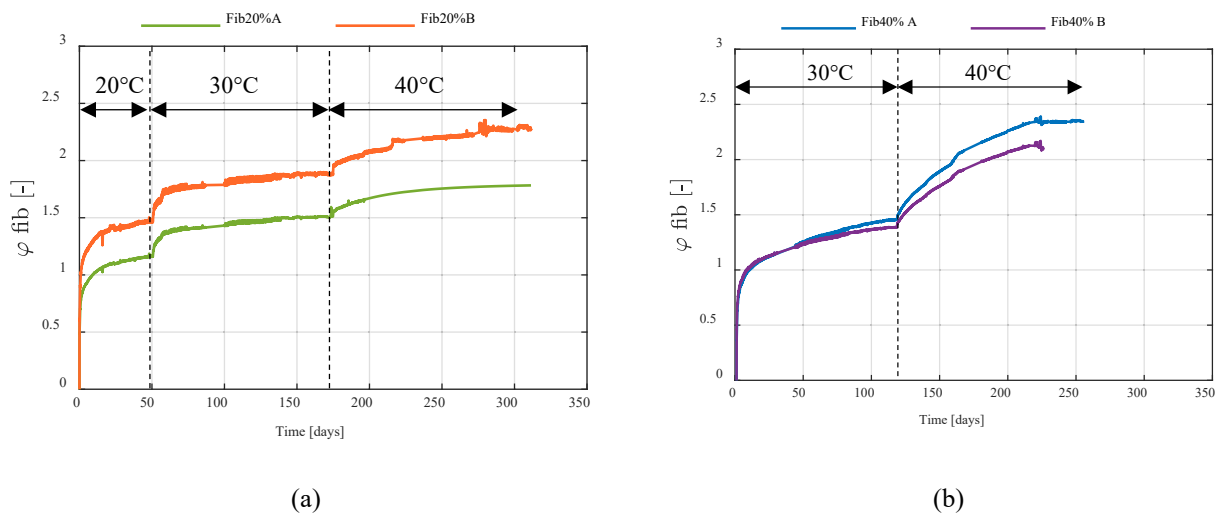

Fig. 15. Fibre tensile creep test: Creep coefficient – time relation for fibers loaded at (a) 20% and (b) 40% of the tensile strength.

Table 4
Cylinders selected for creep tensile test, their residual strength (load), sustained load (creep load) and number of fibers crossing the crack.

Sample ID	Residual force [kN]	Creep Load [kN]	COD$_m$ [mm]	Load ratio [-]	N° Fibers
T5A	7.93	3	0.30	0.38	75
T3A	4.56	3	0.30	0.60	59
T3C	5.38	3	0.30	0.53	80

With this information, a rough estimate of the stress level carried by the fibers across the crack during the long-term test was obtained, by dividing the long-term load applied to each cylinder by its effective number of fibers crossing the crack. The mean stress intensity between the three cylinders corresponded to approximately the 20% of the maximum fibre tensile strength (473 MPa).

4.5. Flexural creep deformations of prims

According to the procedure described in section 2.4.5, 8 prisms were pre-cracked until a crack mouth opening displacement (CMOD) of 0.5 mm, in order to activate the MS fibres; Fig. 21 showed the force-CMOD curves for all specimens. Three of them were chosen for the following creep tests according to the higher residual strength criterium (thicker solid curves in Fig. 21). In any case, the dispersion of results was

expected and acceptable.

In Table 5 the values of the residual strength, in terms of load, for each specimen are indicated, together with the applied sustained load, indicated as creep load, and the corresponding load ratio. Given the different load scheme from the pre-cracking to creep phase, three-point bending to four-point bending, the long-term load was computed so to have the same bending moment value in both configurations.

The deformations measured during the creep flexural tests were presented in terms of development with time of CMOD and creep coefficient – $\varphi_f = (\varepsilon_{visc} - \varepsilon_{inst}) / \varepsilon_{inst}$ (computed as described in the previous section identifying the elastic deformation) – in Fig. 22 and Fig. 23, respectively.

Like in previous tests, after first instantaneous loading, long-term curves presented a slope reducing with time and a sudden increase of slope immediately after each temperature increase; unlike previous tests, the slope reduction after more than nine months of continuous loading was much smaller and the global behaviour was not expected to have reached a steady state condition (linear increase with time in log-scale). Considering a time step of 1 day, the slope measured after the first increment of temperature is of 2%, compared with 0.8% when passing from 30 °C to 40 °C.

The three specimens considered, provided for very homogeneous results, both under instantaneous and long-term loadings, at least when compared with scattering of results from previous tests; the explanation of this was that they were chosen among a number of pre-cracked prisms
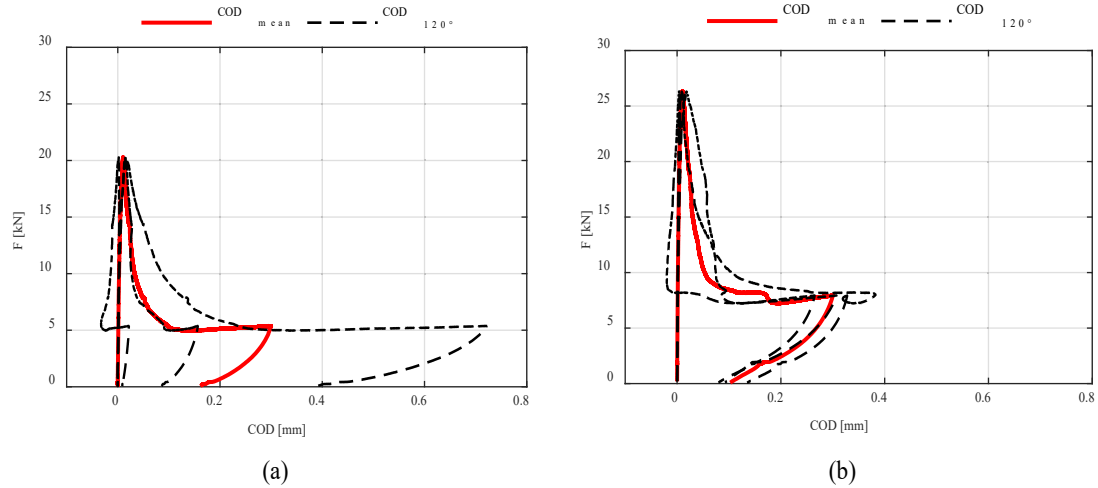
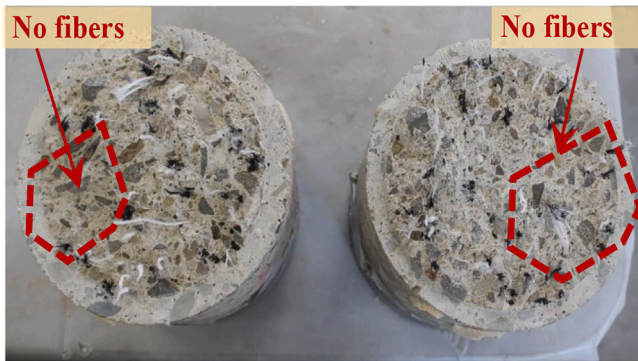**Fig. 16.** Force – COD of pre-cracking tensile test for (a) T3C sample; (b) T5A sample;

Fig. 17. Fibers distribution on cracked surface of T3C cylinder.
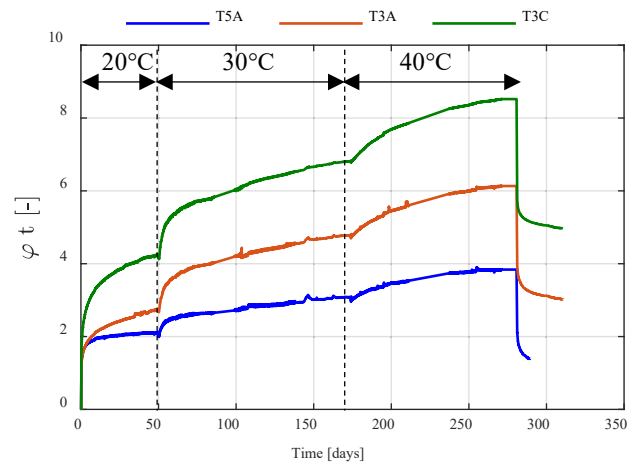

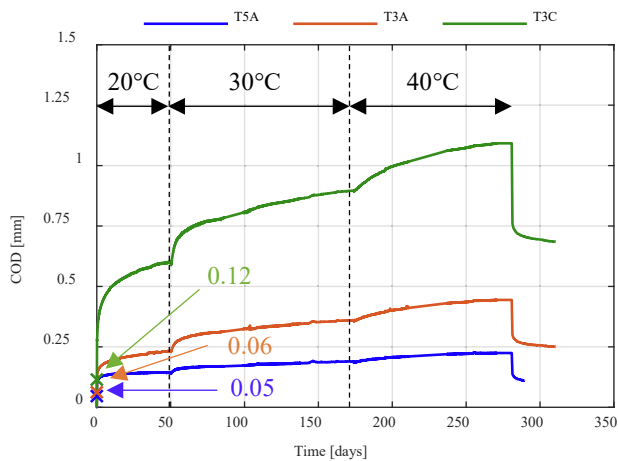**Fig. 19.** Uniaxial tensile test creep coefficient (in terms of crack opening) – time relation.

Fig. 18. Uniaxial tensile creep test COD – time relation.

Fig. 20. Load – COD curve including all phases of the uniaxial tensile creep test.

and, even more important, the cracked surface was larger than that of the cylinders, thus allowing for a larger and more stable number of fibers crossing it.

In terms of creep coefficient, prisms reached a maximum value of approximately 4.5, which is larger than that coming from the long-term concrete behaviour, similar to that of single fibers and smaller than that from cylinder under tensile forces. This remark confirmed that the long-
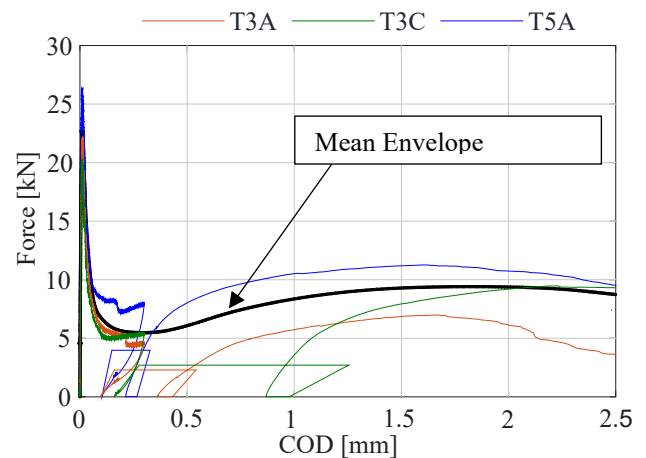
Fig. 21. Pre-cracking test: Force – CMOD curves.

Fig. 23. Flexural test creep coefficient (in terms of crack opening) – time relation.

Table 5
Prisms selected for creep flexural test, residual strength (load), sustained applied load, load ratio and number of fibers crossing the crack.

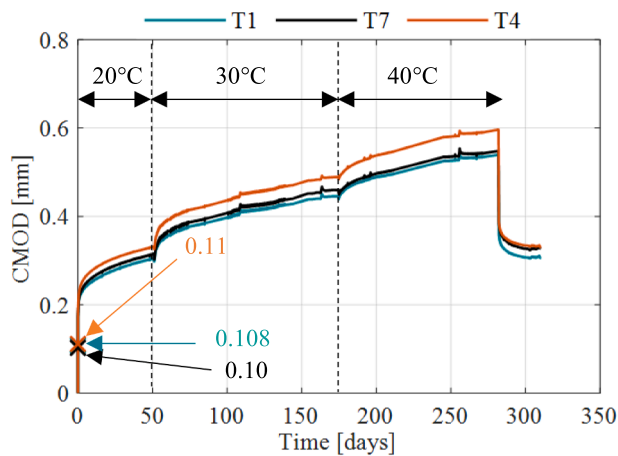| Sample ID	Residual force [kN]	Creep Load [kN]	COD$_m$ [mm]	Load Ratio [-]	N° Fibers
T1	9.66	6.91	0.50	0.51	121
T4	8.36	6.91	0.50	0.49	118
T7	9.46	6.91	0.50	0.51	111

Fig. 22. Flexural creep test CMOD – time relation.

term behaviour of MSFRC under flexure can be obtained as a combination of the creep of concrete, viscous behaviour of fibres and of a further contribution due to fiber-concrete long term bond.

After unloading, the CMOD was measured for 30 more days: the load removal produced a large CMOD recovery, while the period at rest provided for a reduced further recovery, well established at the end of the measurement period.

Finally, all the specimens were reloaded until failure: in Fig. 24, the dark blue curves describe the behaviour of the specimens reloaded to failure after the pre-cracking, where the outliers were excluded; the red curves describes the behaviour of the specimens subjected to creep (like for cylinders – Fig. 20) and the light blue curve the mean short-term behaviour of eight prisms tested in bending in one single phase (filled light blue area). The black solid line represents the ideal average behaviour of the red curves; it seems to be not particularly affected by
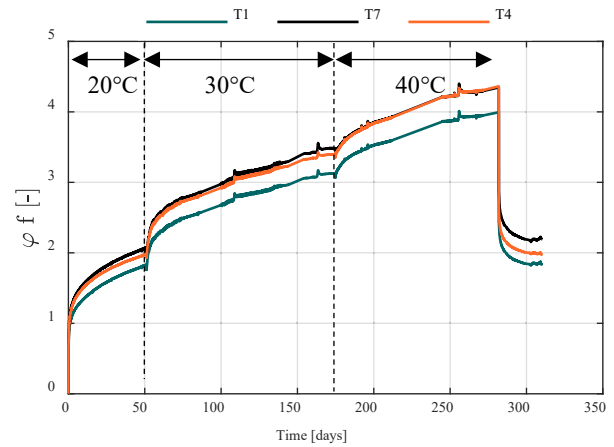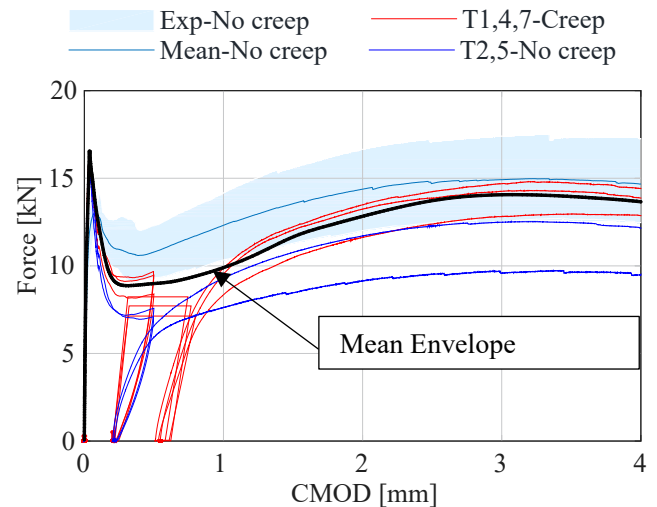

Fig. 24. Load – CMOD curve including the main phases of the flexural creep test.

the long-term loading, keeping even in this case, the expected residual capacity (especially for large values of CMOD).

Fig. 25 showed the correlation between the residual strength at CMOD equal to 0.5 and 1.5 mm and the number of fibers crossing the cracked surface: given the reduced number of data, a linear correlation curve was adopted to interpolate experimental results both from specimens subjected to 28 days short-term loading or at least subjected to test late (blue points) and from specimens subjected to long-term conditions (red crosses). As expected, the level of correlation is good and the possible reduction of mechanical performances due to the long-term loading was not so appreciable. As a confirmation, given the same number of fibres, some points and crosses are really close, suggesting the same residual strength.

The complexity of the observed behaviours at the different levels (concrete, fiber, composite systems), suggests the adoption of a numerical model as a necessary tool to better understand the role of each component in term of time-dependent deformations of the global system. Such a model can now be calibrated with the collected experimental results.
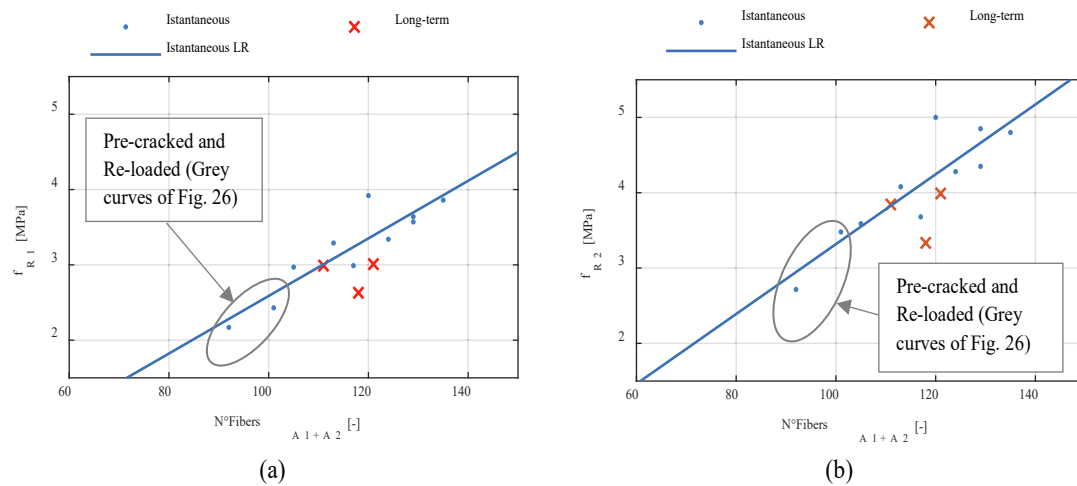
Fig. 25. Linear regression (LR) of (a) f_{R1} (CMOD 0.5 mm) – N fibers; (b) f_{R2} (CMOD 1.5 mm) – N fibers in short- and long-term conditions.

5. Conclusions

The development of the experimental tests allowed to draw the following remarks:

- When conducting fibers tensile creep tests, the key aspects were the reliability of the gripping method and the avoidance of unexpected flexural force component; the former aspect was satisfactorily issued by using bolted steel plates with sand paper in-between; the latter was satisfied by introducing a number of hinges working around orthogonal axis. Repeatability of results showed the robustness of the technique.
- Results of tensile creep tests on cracked MSFRC cylinders were mainly influenced by the fibers' dispersion, which can be modified by the concrete casting process and by the dimensions of the considered specimen. To this purpose and to maintain the similarity with the conditions of the portion of the prisms under traction, cylinders were cored directly from the prisms along their longitudinal direction and they were given the largest possible diameter size. Even in this case, a remarkable dispersion of results was obtained, leading to the necessity of considering a large number of specimens for the selection of a more homogeneous subset for the mechanical behaviour characterization.
- The analysis of the results made possible to draw the following conclusions:
- All the measured creep curves, irrespective of the type of tests they came from, showed a sudden slope increase when the temperature was increased; the slope variation was smaller as the longer the time under load.
- The tensile creep tests on notched pre-cracked cylinders allowed to observe the coupling between the creep of single fibers and the fibre-to-matrix long-term bond behaviour. Although the estimated force level carried by the single fibre in this test was consistent with the force level considered in the fibre creep test (20% of strength), the corresponding creep coefficients were remarkably different, suggesting that the role played by the fibre-to-matrix bond (or slippage) was fundamental to govern the long-term behaviour of fibres embedded into cracked concrete.
- After more than 9 months under constant loading and with two temperature increments, the tests carried out provided for different values of creep coefficients: $1 \div 1.5$ for concrete creep tests, $2 \div 3$ for tensile creep tests on fibers, $4 \div 8$ for tensile creep tests on cracked cylinders and $4 \div 4.5$ for long-term bending on prisms. Particular care should be used when considering creep coefficients from tensile creep tests on cylinders, since uneven fibres distribution can easily produce high and scattered values.

- The comparison of the creep curves from all the tests developed, made it possible to identify the principal mechanisms driving the long-term flexural behaviour of MSFRC prisms: the viscous elongation of macro-synthetic fibres together with their long-term slippage inside the surrounding concrete appeared to be the most important aspects; the remarkably smaller viscosity of concrete in compression, on the contrary, played a secondary role, consisting of slowing down the neutral axis position translation toward the most compressed part of the prism.
- In order to understand if and how the long-term loading could affect the mechanical capacity of MSFRCs, at the end of the time under loading, both cylinders and prisms were subject to instantaneous loading till failure; results suggested that the long-term loading (to the considered extent) was not able to appreciably reduce the mechanical capacity of the systems while, on the contrary, a remarkable increase of deformation and crack opening was observed.
- Even if few data from long-term loading on prisms were available, the tests carried out confirmed that the correlation between the number of fibers crossing the crack and the residual strength still holds.
- Given the similarity in flexural creep behaviour (Fig. 23), the experimental results may provide further insight into the subject that will shed light on how larger structural elements, that are generally subjected to bending forces and therefore to combined compressive and tensile creep effect, will behave.
- The results made available through the present experimental campaign will allow the development of a detailed numerical model able to predict the long-term behaviour of MSFRC elements, since its elementary mechanisms will be calibrated in terms of both instantaneous and viscous behaviour of different components.

Declaration of Competing Interest

The authors declare that they have no known competing financial interests or personal relationships that could have appeared to influence the work reported in this paper.

References

[1] T.C. Easley, K.T. Faber, S.P. Shah, Use of a Crack-Bridging Single-Fiber Pullout Test to Study Steel Fiber/Cementitious Matrix Composites, J. Am. Ceram. Soc. 82 (12) (2010) 3513–3520.

[2] W. Lin, Y. Teruhiko, Chapter Seven - Steel Bridges, Bridge Engineering (2017) 111–136.

[3] V. Guerini, A. Conforti, G.A. Plizzari, S. Kawashima, Influence of steel and macro-synthetic fibers on concrete properties, Fibers 6 (3) (2018) 47.

[4] M.G. Alberti, A. Enfedaque, J.C. Gálvez, A. Picazo, Recent advances in structural fibre-reinforced concrete focused on polyolefin-based macro-synthetic fibres, Mater. Construcción 70 (337) (2020) 206.

[5] R. Babaie, M. Abolfazli, A. Fahimifar, Mechanical properties of steel and polymer fiber reinforced concrete, J. Mech. Behav. Mater. 28 (1) (2019) 119–134.

[6] O.S. Abiola Natural fibre cement composites, in Advanced High Strength Natural Fibre Composites in Construction 2017 205 214.

[7] X. Zhou, H. Saini, and G. Kastiukas, Engineering Properties of Treated Natural Hemp Fiber-Reinforced Concrete, Front. Built Environ., vol. 3, no. 33, 2017.

[8] BS EN 14651-2005, Test method for metallic fibred concrete — Measuring the flexural tensile strength (limit of proportionality (LOP), residual, Br. Stand. Inst., vol. 3, pp. 1–17, 2005.

[9] CNR-DT 204/2006, Istruzioni per la Progettazione , l ' Esecuzione ed il Controllo di Strutture Consiglio Nazionale delle Ricerche, 2008.

[10] D.M. 17 Gennaio 2018, Norme Tecniche per le costruzioni (NTC2018), Ministero delle Infrastrutture e dei Trasporti, 2018.

[11] Circolare 21 Gennaio 2019, Istruzioni per l'applicazione dell'«Aggiornamento delle 'Norme tecniche per le costruzioni'» di cui al decreto ministeriale 17 gennaio 2018., Ministero delle Infrastrutture e dei Trasporti, 2019.

[12] N. Buratti, C. Mazzotti, M. Savoia, Post-cracking behaviour of steel and macro-synthetic fibre-reinforced concretes, Constr. Build. Mater. 25 (5) (2011) 2713–2722, https://doi.org/10.1016/j.conbuildmat.2010.12.022.

[13] D. Ciancio, C. Mazzotti, N. Buratti, Evaluation of fibre-reinforced concrete fracture energy through tests on notched round determinate panels with different diameters, Constr. Build. Mater. 52 (2014) 86–95, https://doi.org/10.1016/j.conbuildmat.2013.10.079.

[14] Q. Zhao, J. Y., G. Guoqing, J. Jinyang, and L. Xiaochen, Effect of fiber types on creep behavior of concrete, Constr. Build. Mater., vol. 105, pp. 416–422, 2016.

[15] E. Bernard, Creep of cracked fibre reinforced shotcrete panels, Shotcrete More Eng. Dev. (2004) 47–57.

[16] G. Plizzari and P. Serna, Structural effects of FRC creep, Mater. Struct., vol. 51, no. 167, 2018.

[17] G. Zhao, M. di Prisco, L. Vandewalle, Experimental investigation on uniaxial tensile creep behavior of cracked steel fiber reinforced concrete, Mater. Struct. 48 (10) (Oct. 2015) 3173–3185, https://doi.org/10.1617/s11527-014-0389-1.

[18] M. Hunger, J. Bokern, S. Cleven, R. Vrijdaghs, Creep in FRC –, From Material Properties to Composite Behavior (2021).

[19] John D. Ferry, Viscoelastic Behaviour of Polymers, in Physicochemical Behavior and Supramolecular Organization of Polymers, 2009.

[20] N. Buratti and C. Mazzotti, Temperature effect on the long term behaviour of macro-synthetic-and-steel–fibre reinforced concrete, 2012.

[21] F.-J. Wortmann, K.V. Schulz, Stress relaxation and time/temperature superposition of polypropylene fibres, Polymer (Guildf) 36 (2) (1995) 315–321.

[22] D. Lopez, S. Thuillier, Y. Grohens, Prediction of elastic anisotropic thermo-dependent properties of discontinuous fiber-reinforced composites, J. Compos. Mater. 54 (14) (2020) 1913–1923.

[23] C. Stern, On the performance of polypropylene: between synthesis and end-use properties. 2005.

[24] D. Pedrazzoli, A. Pegoretti, Long-term creep behavior of polypropylene/fumed silica nanocomposites estimated by time–temperature and time–strain superposition approaches, Polym. Bull. 71 (9) (2014) 2247–2268.

[25] C. Vipulanandan, Y.J. Ahossin Guezo, Effects of temperature and strain rate on the tensile behavior of polypropylene composites insulator coatings used in offshore deepwater pipelines, J. Appl. Polym. Sci. 134 (36) (2017) 45209.

[26] M. Yongfeng, G. Strobl, and P. Wette, Change of modulus and yielding properties of syndiotactic polypropylene with the glass transition, e-Polymers, vol. 2, no. 1, 2002.

[27] P. Pujadas, A. Blanco, S. Cavalaro, A. de la Fuente, A. Aguado, The need to consider flexural post-cracking creep behavior of macrosynthetic fiber reinforced concrete, Constr. Build. Mater. 149 (2017) 790–800.

[28] N. Buratti, C. Mazzotti, Creep testing methodologies and results interpretation, vol. 14, Springer, Dordrecht, 2017.

[29] A. Llano-Torre and P. Serna, Recommendation of RILEM TC 261-CCF: test method to determine the flexural creep of fibre reinforced concrete in the cracked state, Mater. Struct. Constr., vol. 54, no. 3, 2021, doi: 10.1617/s11527-021-01675-0.

[30] A. Llano-Torre et al., Statements and Conclusions, vol. 34. 2021.

[31] A. Llano-Torre et al., Analysis of the RRT Results, vol. 34. 2021.

[32] E. García-Taengua, S. Arango, J.R. Martí-Vargas, P. Serna, Flexural creep of steel fiber reinforced concrete in the cracked state, Constr. Build. Mater. 65 (2014) 321–329, https://doi.org/10.1016/j.conbuildmat.2014.04.139.

[33] B.E. Barragán, R. Zerbino, Creep behaviour of cracked steel fibre reinforced concrete beams, in: 7th RILEM Symposium on Fibre Reinforced Concrete BEFIB2008, 2008, pp. 577–586.

[34] A. Llano-Torre, J.R. Martí-Vargas, P. Serna, Flexural and compressive creep behavior of UHPFRC specimens, Constr. Build. Mater. 244 (2020), 118254, https://doi.org/10.1016/j.conbuildmat.2020.118254.

[35] D.H. Monetti, et al., Long-term behavior of cracked fiber reinforced concrete under service conditions, Constr. Build. Mater. 196 (2019) 649–658, https://doi.org/10.1016/j.conbuildmat.2018.10.230.

[36] E. Vasanelli, F. Micelli, M.A. Aiello, G.A. Plizzari, M. Molfetta, Creep and durability aspects of ordinary reinforced FRC beams, Proc, in: 2nd Work. new boundaries Struct. Concr, 2011, pp. 143–149.

[37] E. Vasanelli, F. Micelli, M. A. Aiello, and G. Plizzari, Long term behaviour of fiber reinforced concrete beams in bending, Eighth RILEM Int. Symp. Fibre Reinf. Concr. (BEFIB 2012)(Guimarães, Bagneux, Univ. do Minho, pp. 1–12, 2012.

[38] E. Vasanelli, F. Micelli, M.A. Aiello, G. Plizzari, Long term behavior of FRC flexural beams under sustained load, Eng. Struct. 56 (2013) 1858–1867.

[39] N. Buratti, C. Mazzotti, Experimental tests on the effect of temperature on the long-term behaviour of macrosynthetic Fibre Reinforced Concretes, Constr. Build. Mater. 95 (2015) 133–142.

[40] R. Vrijdaghs, M. Di Prisco, L. Vandewalle, Creep of cracked polymer fiber reinforced concrete under sustained tensile loading, in: in 9th International Conference on Fracture Mechanics of Concrete and Concrete Structures FraMCoS-9, 2016, pp. 1–9.

[41] G. Zhao, M. Di Prisco, and L. Vandewalle, Experimental Research and Numerical Simulation of Post-Crack Creep Behavior of SFRC Loaded in Tension, in Mechanics and Physics of Creep, Shrinkage, and Durability of Concrete - Proceedings of the Ninth International Conference on Creep, Shrinkage, and Durability Mechanics (CONCREEP-9), 2013, pp. 340–347, doi: 10.1061/9780784413111.040.

[42] A.J. Babafemi, A. du Plessis, W.P. Boshoff, Pull-out creep mechanism of synthetic macro fibres under a sustained load, Constr. Build. Mater. 174 (2018) 466–473.

[43] R. Vrijdaghs, M. di Prisco, L. Vandewalle, Creep Deformations of Structural Polymeric Macrofibers, in Creep Behaviour in Cracked Sections of Fibre Reinforced Concrete, RILEM Bookseries, Springer, Dordrecht 14 (2017) p.

[44] M. Jiràsek, Z.P. Bazant, Inelastic Analysis of Structures, Wiley, 2002.

[45] B.S. En, 14845–1:2006, Test methods for fibres in concrete - Part 1, Reference concretes. (2006).

[46] S. Arango, E. Taengua, J. R. M. Vargas, and P. S. Ros, a Comprehensive Study on the Effect of Fibers and Loading on Flexural Creep of Sfrc, Befib, pp. 1–11, 2012.

[47] UNI EN 12390-3:2019, Prove sul calcestruzzo indurito - Parte 3:Resistenza alla compressione dei provini. 2019.

[48] UNI EN 12390-13:2013, Prove sul calcestruzzo indurito - Parte 13: Determinazione del modulo di elasticità secante in compressione. 2013.

[49] B. E. Barragán, R. Gettu, M. a. Martín, and R. L. Zerbino, Uniaxial tension test for steel fibre reinforced concrete—a parametric study, Cem. Concr. Compos., vol. 25, no. 7, pp. 767–777, 2003, doi: https://doi.org/10.1016/S0958-9465(02)00096-3.

[50] C. Del Prete, N. Buratti, S. Manzi, and C. Mazzotti, Macro-synthetic fibre reinforced concrete: influence of the matrix mix design on interfacial bond behaviour, 2019.

[51] S. Arango, E. G. Taungua, J. R. M. Vargas, and P. Serna Ros, A comprehensive study on the effect of fibers and loading on flexural creep of SFRC, in BEFIB2012 - Fibre reinforced concrete, 2012, pp. 704–715.

[52] R.L. Zerbino, B.E. Barragan, Long-term behavior of cracked steel fiber-reinforced concrete beams under sustained loading, ACI Mater. J. 109 (2) (2012) 215–224.

[53] Eurocode 2 : Design of concrete structures —, vol. 3, 2004.

[54] A.J. Babafemi, W.P. Boshoff, Tensile creep of macro-synthetic fibre reinforced concrete (MSFRC) under uni-axial tensile loading, Cem. Concr. Compos. 55 (2015) 62–69, https://doi.org/10.1016/j.cemconcomp.2014.08.002.